energy&fuels

pubs.acs.org/EF

Article

Molecular Structures of Refractory Sulfur Compounds in Heavy Oil Hydrodesulfurization Characterized by Collision-Induced Dissociation Fourier Transform Ion Cyclotron Resonance Mass Spectrometry

Xinheng Cai, Rong Shi, Wei Wang,* Huandi Hou, Dongyue Peng, Naixin Wang, Zhonghuo Deng, Zelong Liu, and Qundan Zhang

Cite This: *Energy Fuels* 2022, 36, 1326−1337

Read Online

ACCESS | Metrics & More | Article Recommendations | Supporting Information

ABSTRACT: Hydrodesulfurization (HDS) is a widely used technology to reduce the sulfur content of heavy oils, and the HDS reactivities of sulfur compounds are closely related to their structures. In this work, the tandem mass spectra of sulfur-containing model compounds were measured by Fourier transform ion cyclotron resonance mass spectrometry (FT-ICR MS) coupled with collision-induced dissociation. The influences of naphthenic rings, size of aromatic rings, number of heteroatoms, and number of alkyl side chains to the fragmentation behaviors of sulfur-containing model compounds were studied. Finally, the structure differences of sulfur compounds in heavy oils before and after hydrogenation were compared by tandem mass spectra of FT-ICR MS. The most refractory sulfur compounds in the heavy oil were those with fully conjugated aromatic rings attached with fewer and longer side chains. These results would be helpful for the development of a HDS catalyst/process for heavy oils. For example, developing a new HDS catalyst with high alkyl side-chain cracking activity may be conducive to HDS of heavy oils.

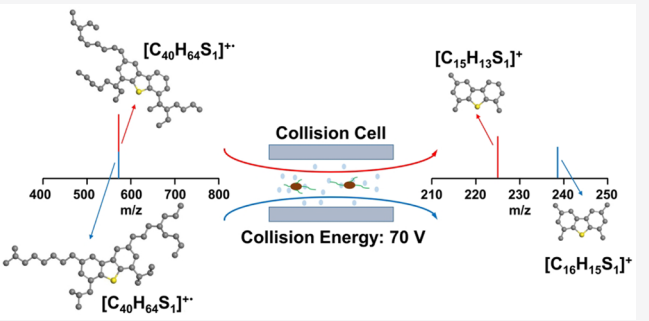

1. INTRODUCTION

Generally, sulfur is the most abundant heteroatom in crude oils, especially in heavy fractions of crude oils.[1] The economic value of crude oils also depends upon the sulfur content. Crude oils with sulfur contents higher than 0.5% are defined as sour crude oils, which are considered as inferior crude oils. On the other side, a series of sulfur regulations have been widely implemented in the world, and the sulfur contents of the clean transportation fuels have been reduced to below 10 ppm.[2,3]

Hydrodesulfurization (HDS) is one of the most important methods to reduce the sulfur content of heavy oils. The HDS efficiency of heavy oils is closely related to the types and structures of sulfur compounds.[4−6] A better understanding about the structure−reactivity relationships of sulfur compounds would be beneficial for the development of a heavy oil desulfurization catalyst/process.[7−9] The refractory sulfur compounds in light oils during HDS have been widely studied,[2,3,10−12] and most of the sulfur exists in the form of thiophene rings. It has been proven that the positions and numbers of the alkyl side chains[3,10,12,13] and the ring structures[14] of sulfur compounds are main factors to the HDS reactivities of sulfur compounds in light gas oils and diesels. However, the complexity of heavy oils increases dramatically with the boiling point, and the low-volatile property of heavy oils also brings difficulties to the detailed analysis of sulfur compounds in heavy oils by conventional gas chromatography methods.

The implementation of high-temperature comprehensive two-dimensional gas chromatography (HT GC × GC) allowed for the detailed characterization of sulfur compounds in vacuum gas oils (VGOs).[15−18] Mass spectrometry (MS) and a sulfur chemiluminescence detector (SCD) were hyphenated with HT GC × GC, providing qualitative and quantitative information on sulfur compounds in VGOs. The combination of GC × GC and high-resolution time-of-flight mass spectrometry was also applied to distinguish the C_3 versus SH_4 mass split in the GC-amenable fraction of crude oil.[19] The mass split of C_3 versus SH_4 is 0.0034 Da, which was typically resolved by ultrahigh-resolution mass spectrometry. Compounds with different elemental compositions as a result of C_3 versus SH_4 were distributed in different regions in GC × GC,

Received: October 14, 2021
Revised: January 6, 2022
Published: January 21, 2022

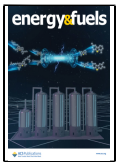

Table 1. Information of the Sulfur-Containing Model Compounds

	CAS No.	Structure		CAS No.	Structure
1	90501-14-7		9	243-68-5	
2	30796-92-0		10	1255308-97-4	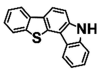
3	31473-75-3		11	153935-93-4	
4	203-42-9	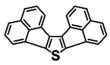	12	959234-20-9	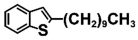
5	17164-77-1	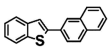	13	1268344-21-3	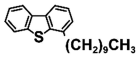
6	241-34-9	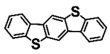	14	——	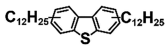
7	241-13-4	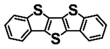	15	——	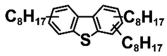
8	251991-63-6				

reducing the mass resolution required to distinguish the C_3 versus SH_4 mass split. However, as a result of the limitation of the suitable temperature range of GC columns, GC × GC was inadequate to detect the sulfur compounds with a high molecular weight in residues.[20−23]

Fourier transform ion cyclotron resonance mass spectrometry (FT-ICR MS) was also applied for the characterization of sulfur compounds in heavy oils, and atmospheric pressure photoionization (APPI) and electrospray ionization (ESI) were currently more suitable ionization methods for the analysis of sulfur compounds or derived sulfur compounds.[1] Sulfur compounds were ionized directly by the APPI source,[24−28] while the derivatization with methyl iodide[24,29,30] or silver cation[21,31] was necessary for the ESI source. The transformations of sulfur compounds during hydroprocessings were studied for the coal tar,[32] shale oils,[33] VGO,[34,35] atmospheric residues,[36−40] and asphaltenes[41−43] by FT-ICR MS. Moreover, the combinations of gel permeation chromatography (GPC),[44] high-performance liquid chromatography (HPLC),[45,46] thermogravimetry (TG),[47−49] and ion mobility (IM)[50−54] with high-resolution mass spectrometry were also applied to obtain more information about the structures of sulfur compounds in heavy oils.

Tandem mass spectrometry has been proven to be an important method for structural characterization of heavy oils.[55−57] As a result of the complexity of petroleum molecules, a clear understanding of the tandem mass spectra of model compounds would be helpful to infer the possible structures of sulfur compounds in heavy oils. Sulfur-containing model compounds with different ring structures and alkyl chains have been studied by mass spectrometers coupled with chemical ionization (CI),[58] atmospheric pressure chemical ionization (APCI),[59,60] ESI,[61] and APPI.[61−63] The loss of a S-containing group (including S atom, CS group, or CHS group) was observed for sulfur model compounds with short side chains or without side chains, while the cleavage of the side chain was the major fragmentation pathway of the model compounds with long side chains. Other types of model compounds with multiple alkyl chains would also be valuable for interpreting the tandem mass spectra of sulfur compounds in heavy oils. Jarrell et al. studied the tandem mass spectra of pyrenes attached with two and four alkyl chains.[64] The cleavage of the side chains generally left a methylene group (CH_2) or methyl group (CH_3) on the pyrene ring. For pyrene substituted with two alkyl chains, the loss of methyl was not observed. However, for pyrene substituted with four alkyl chains, a significant loss of the methyl group was observed. Ha et al. found that the fragmentation patterns of isomers with different numbers of alkyl side chains were quite different.[65] Nyadong et al. reported the tandem mass spectra of hexa-*peri*-hexabenzocoronene with six dodecyl groups obtained by the hybrid linear ion trap Orbitrap (LTQ Orbitrap).[66] Both collision-induced dissociation (CID) mode and high-energy collision-induced dissociation (HCD) mode were applied, and complete dealkylation was only observed at HCD mode. It should be noted that there are two collision cells in LTQ Orbitrap. When the collision energy is applied in the linear ion trap, it is called CID mode. When the collision energy is applied in the HCD collision cell, it is called HCD mode. Wittrig et al. reported the tandem mass spectra of 1-phenyl-9*H*-carbazole derivatives attached with two alkyl chains.[67] It was found that the aromatic core remained unchanged while a series of alkyl losses was observed in the CID spectra.

In this work, CID spectra of 15 sulfur-containing model compounds were studied at different collision energies by APPI FT-ICR MS. With the increase of collision energies from 30 to 90 V, almost complete cleavage of alkyl side chains could be achieved for model compounds substituted with multiple side chains. Model compounds containing multiple S atoms (S_x species, where $x \geq 2$) may easily lose some of the S atoms at high collision energies, while S_1 model compounds were more resistant at high collision energies. The losses of the C_2 group were observed for most model compounds at collision energies of 70 and 90 V. Finally, the CID spectra of an

https://doi.org/10.1021/acs.energyfuels.1c03534
Energy Fuels 2022, 36, 1326−1337

atmospheric residue and its HDS product were compared at different collision energies, and the structural features of refractory heterocyclic sulfur compounds during the HDS processes were suggested.

2. EXPERIMENTAL SECTION

2.1. Chemicals. The information on the sulfur-containing model compounds (**1**−**15**) is shown in Table 1. Some related aromatic hydrocarbon model compounds (**A1**−**A5**) are shown in Table S1 of the Supporting Information. Compounds **1**, **2**, **4**, **8**, **9**, **11**, **12**, and **13** were purchased from Prof. Jan T. Andersson (University of Münster, Germany). Compounds **3** and **5**−**7** were synthesized by Prof. Qitao Tan (Shanghai University, China).[68] Compounds **10** and **A1**−**A3** were purchased from Beijing Innochem Science & Technology Corporation. Compounds **14** and **15** were synthesized by the Friedel−Crafts reaction with methanesulfonic acid as the catalyst,[69] and more details could be found in the Supporting Information. Compounds **A4** and **A5** were synthesized by the co-author Dongyue Peng.

Table 2. Bulk Properties of the Feedstock and Hydrotreating Product

property	SA-AR	SA-AR-HT
density (20 °C) (g cm^{-3})	0.9747	0.9151
Conradson carbon residue (wt %)	10.34	3.64
elemental composition (wt %)		
C	84.30	86.95
H	11.06	12.34
S	4.18	0.39
N	0.24	0.13
metal content (μg g^{-1})		
Ni	21.1	3.1
V	60.5	3.5
SARA fraction (wt %)		
saturates	31.0	54.7
aromatics	46.8	33.2
resins	18.8	11.9
asphaltenes	3.4	0.2

An atmospheric residue from Saudi Arabia (SA-AR) served as the feedstock. HDS of SA-AR was conducted in a microreactor. The catalyst was NiO/MoO_3 supported on alumina; the operating temperature was 380 °C; the hydrogen pressure was 15.0 MPa; the liquid hourly space velocity (LHSV) was 0.20 h^{-1}; and the H_2/feed ratio was 700:1 (m^3/m^3). The product of SA-AR were named SA-AR-HT. The bulk properties of SA-AR and SA-AR-HT are shown in Table 2. Saturate, aromatic, resin, and asphaltene (SARA) fractions were separated and measured on the basis of ASTM D2007 and NB/SH/T 0509.

2.2. FT-ICR MS Analysis. The model compounds and petroleum samples were dissolved in toluene (HPLC grade). The model compounds were diluted to 0.001−0.005 mg/mL, and the petroleum samples were diluted to 0.5 mg/mL by toluene. The prepared samples flowed through a fused-silica capillary at a rate of 360 μL/h by a syringe pump (Hamilton Corporation). Analyses were conducted on 15 T Bruker SolariX XR FT-ICR MS. The ionization source was positive-mode APPI. Nitrogen (99.999%) served as the drying gas and nebulizing gas. The collision gas was argon (99.999%). The drying gas flow rate was 2.0 L/min at the temperature of 200 °C. The nebulizing gas flow rate was 1.0 L/min. The temperature of the APPI source was set to 400 °C. The skimmer voltage was 15 V. The m/z range was from 100 to 1000 Da for the broadband mass spectra. The radio frequency (RF) amplitudes of the collision hexapole were 500 V_{pp}. The time of flight was 1.0 ms. The data size was 8 M, and time-domain data sets were 128 scans.

For tandem mass spectra, the RF amplitude of the collision hexapole was turned to 1400 V_{pp}. The ions were isolated in the quadrupole, and the isolation width is 1 Da, which was realized by the quadrupole. The CID was performed in the collision cell of the instrument. The collision gas was argon (99.999%), and the pressure was about 3−6 × 10^{-6} mbar. The ions were accumulated for 1.0 s (model compounds) or 2.0 s (heavy oil samples) in the collision cell and then introduced to the ICR cell. The time of flight was 0.8 ms. The collision energies varied from 30 to 90 V. The m/z range was from 50 to 1000 Da.

2.3. Data Analysis. The peaks with a relative abundance higher than six standard deviations of the baseline root-mean-square noise (6σ) were used for the data analysis. Chemical formulas ($C_cH_hN_nO_oS_s$, where $c \leq 100$, $h \leq 200$, $n \leq 4$, $o \leq 4$, and $s \leq 4$) were obtained according to the m/z values, and the relative deviation between the measured m/z and theoretical m/z was lower than 1 ppm. Double bond equivalent (DBE) was calculated as DBE = $c - h/$

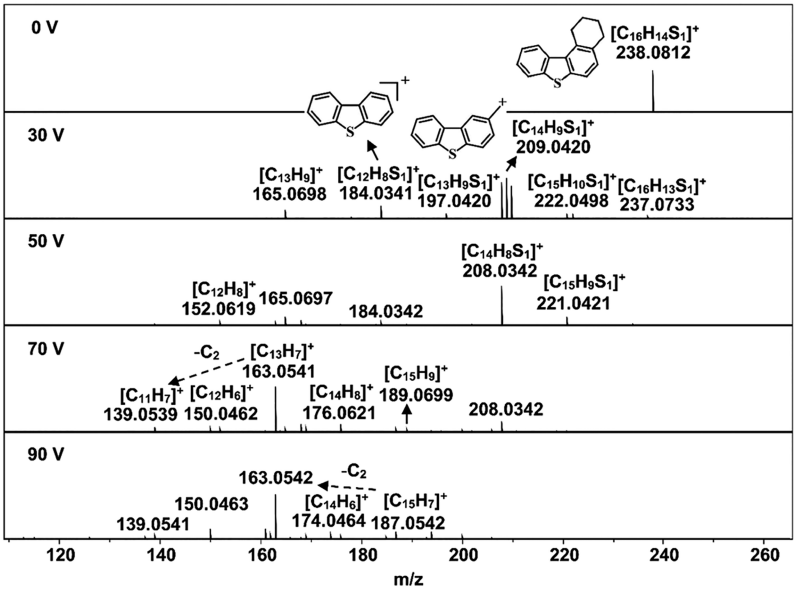

Figure 1. Tandem mass spectra of 1,2,3,4-tetrahydrobenzo[b]naphtho[1,2-d]thiophene (**1**).

https://doi.org/10.1021/acs.energyfuels.1c03534
Energy Fuels 2022, 36, 1326−1337

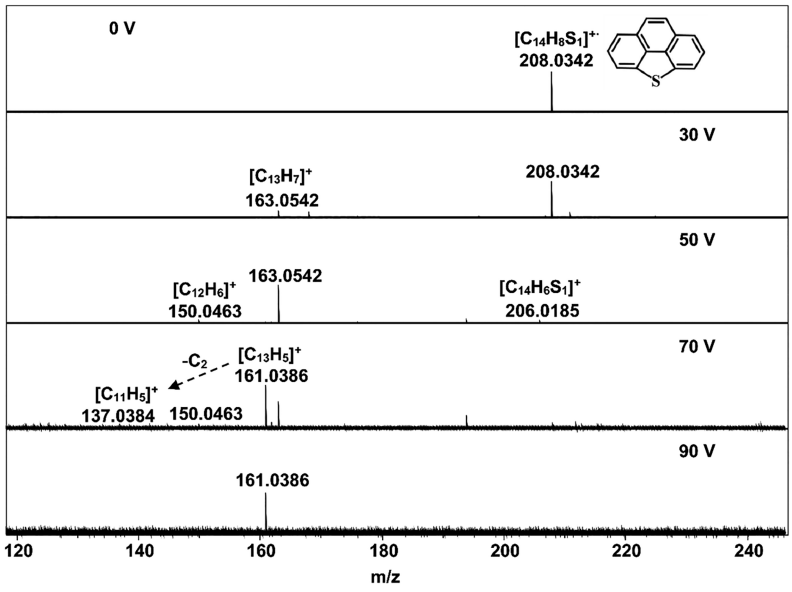

Figure 2. Tandem mass spectra of phenanthro[4,5-*bcd*]thiophene (**2**).

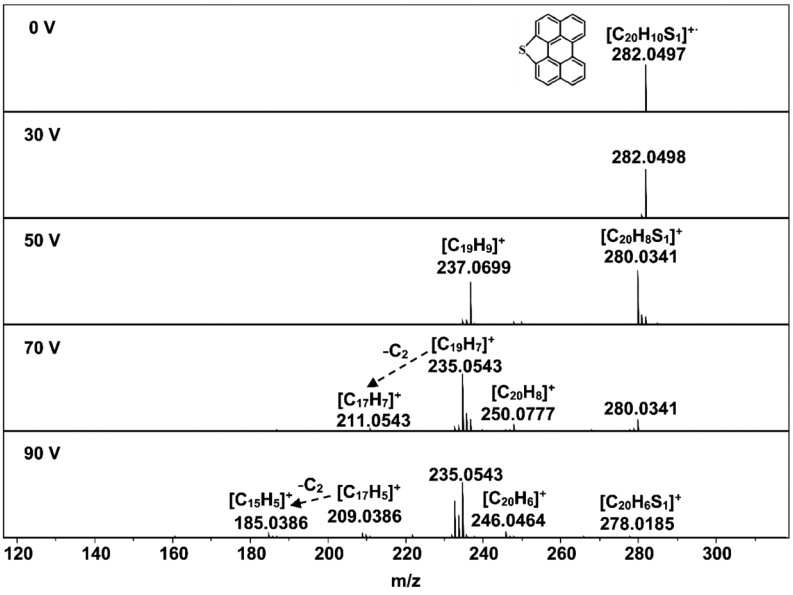

Figure 3. Tandem mass spectra of perylo[1,12-*bcd*]thiophene (**3**).

$2 + n/2 + 1$ for the parent ions, where *c*, *h*, and *n* indicate the numbers of C, H, and N atoms in the formulas. The chemical formulas of the fragment ions were transferred to the corresponding neutral form before calculating the DBE of the fragment ions. The fragment ions with the form of $[M - H]^+$ were dominant at low collision energies, and the *m*/*z* values were mainly odd for sulfur compounds and hydrocarbons. However, both odd and even fragment ions were observed at higher collision energies.

3. RESULTS AND DISCUSSION

3.1. Aromatic Model Compounds Containing One S Atom. The CID spectra of 1,2,3,4-tetrahydrobenzo[*b*]-naphtho[1,2-*d*]thiophene (**1**) are shown in Figure 1. The opening of the naphthenic ring occurred at the collision energy of 30 V, resulting in fragment ions of $[C_{13}H_9S_1]^+$ and $[C_{12}H_8S_1]^+$. The tandem mass spectra of phenanthro[4,5-*bcd*]thiophene (**2**), perylo[1,12-*bcd*]thiophene (**3**), and diacenaphthothiophene (**4**) are shown in Figures 2−4. It was found that the loss of S atoms and CHS groups was restrained at the same collision energy when the model compounds changed from four aromatic rings (compound **2**) to seven aromatic rings (compound **4**). At relatively high collision energies of 70 and 90 V for compounds **1**−**4**, the losses of the C_2 group were widely observed and the *m*/*z* differences of these fragment ions were very close to 24.0000, as shown in Figures 1−4. The C_2 losses were also found in the tandem mass spectra of polycyclic aromatic hydrocarbons (PAHs) before.[70]

Phenyl derivatives of polycyclic aromatic compounds were found in shale oils.[71] Sulfur compounds containing aryl−aryl bonds may also exist in crude oils. The tandem mass spectra of 2-(2′-naphthyl)benzothiophene (**5**) are shown in Figure 5. The aryl−aryl bond was stable at the collision energy of 30 V, and only a slight loss of S atom or CHS group occurred. With

https://doi.org/10.1021/acs.energyfuels.1c03534
Energy Fuels 2022, 36, 1326−1337

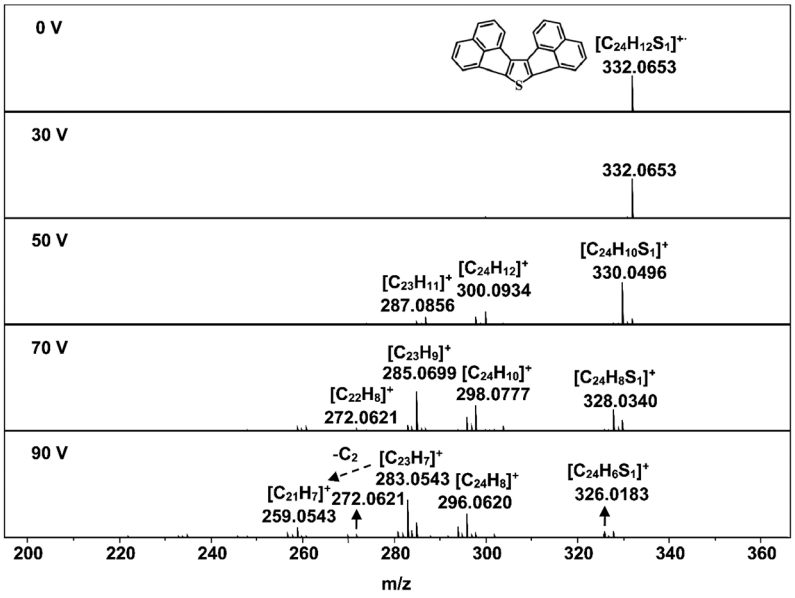

Figure 4. Tandem mass spectra of diacenaphthothiophene (**4**).

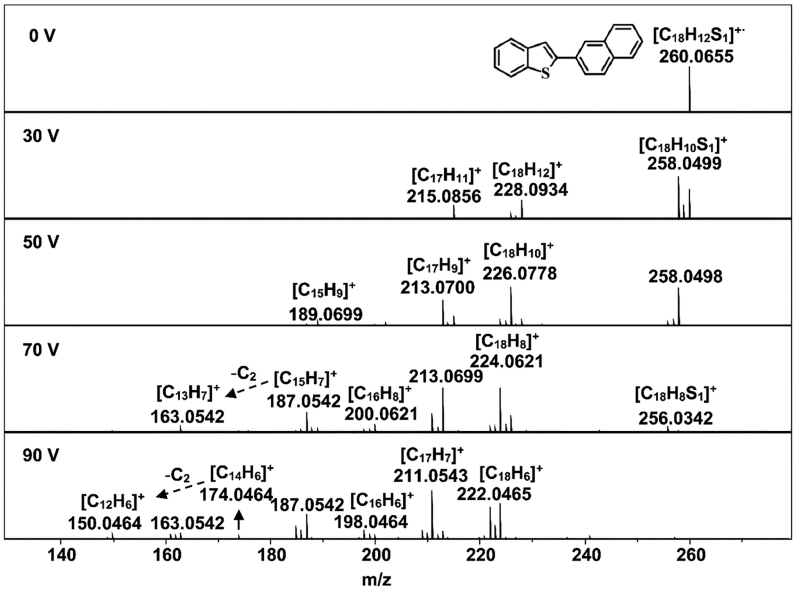

Figure 5. Tandem mass spectra of 2-(2′-naphthyl)benzothiophene (**5**).

the increase of collision energy, the cleavage of the aryl−aryl bond was not observed. However, the aryl−aryl bonds were cleaved at a low collision energy of 30 V for model compounds with larger aromatic rings (≥3 rings), such as 1,3,5-tri(1-naphthyl)benzene (**A1**), 1,3,6,8-tetraphenylpyrene (**A2**), and 9,10-di(naphthalen-2-yl)anthracene (**A3**), illustrated in Figures S2 and S3 of the Supporting Information. Similar result was observed for the model compound rubrene as reported before.[72]

3.2. Sulfur Model Compounds Containing Multiple Heteroatoms. Model compounds benzo[1,2-*b*:4,5-*b*′]bis[1]-benzothiophene (**6**), thieno[3,2-*b*:4,5-*b*′]bis[1]-benzothiophene (**7**), and triphenyleno[1,12-*bcd*:4,5-*b*′*c*′*d*′:8,9-*b*″*c*″*d*″]trithiophene (**8**) stand for the model compounds containing two S atoms and three S atoms, respectively. The tandem mass spectra of compounds **6**−**8** are shown in Figures 6 and 7 and Figure S5 of the Supporting Information. Possible structures of fragment ions from compound **7** are illustrated in Figure S6 of the Supporting Information. There was only a minor loss of S atoms at the collision energy of 30 V for these sulfur compounds with larger aromatic rings, which is quite different from the smaller S_3 model compounds containing only three thiophene rings.[63] One possible reason may be that the thiophene rings in model compounds **6**−**8** are shielded by adjacent aromatic rings. The losses of S atoms and CHS groups occurred at collision energies above 50 V for model compounds **6**−**8**. The C_2 losses also turned to be notable at collision energies of 70 and 90 V.

Model compounds benzo[4,5]thieno[3,2-*b*]quinoline (**9**), 5*H*-benzo[4,5]thieno[3,2-*c*]carbazole (**10**), and benzo[4,5]-thieno[2,3-*c*]naphtho[1,2-*f*]quinoline (**11**) stand for S_1N_1 species. The tandem mass spectra of these model compounds are presented in Figures 8 and 9 and Figure S8 of the Supporting Information. Possible structures of fragment ions

https://doi.org/10.1021/acs.energyfuels.1c03534
Energy Fuels 2022, 36, 1326−1337

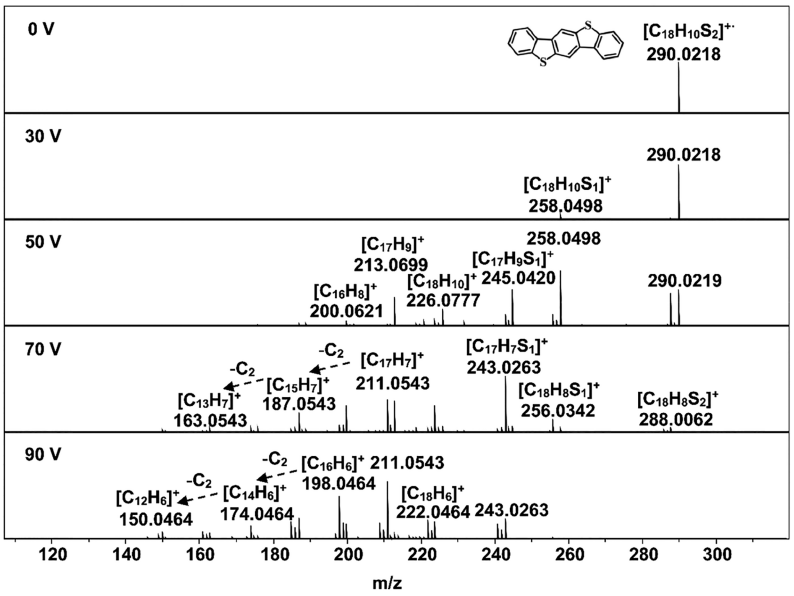

Figure 6. Tandem mass spectra of benzo[1,2-*b*:4,5-*b*′]bis[1]benzothiophene (**6**).

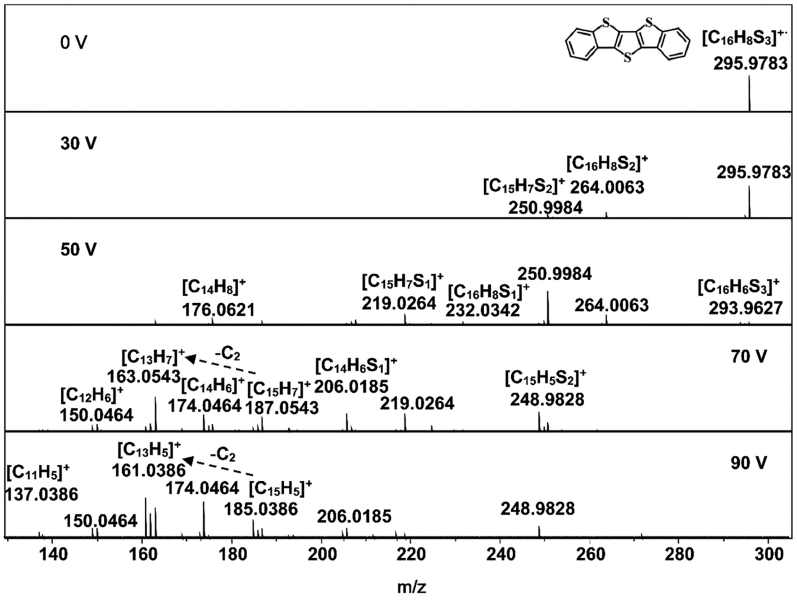

Figure 7. Tandem mass spectra of thieno[3,2-*b*:4,5-*b*′]bis[1]benzothiophene (**7**).

from compound **10** are illustrated in Figure S7 of the Supporting Information. For compound **9**, the loss of S atom was detected at the collision energy of 30 V and the loss of N atom occurred at collision energies above 50 V. This may be due to the bond strength of C−S being weaker than that of C−N. For compounds **10** and **11** with larger aromatic rings, the S and N atoms were very stable at the collision energy of 30 V. The loss of S atom started at the collision energy of 50 V, while the loss of N atom began at the collision energy of 70 V in compounds **10** and **11**. The C_2 losses were detected at collision energies of 70 and 90 V for these S_1N_1 compounds.

3.3. Model Compounds Attached with Alkyl Side Chains. The tandem mass spectra of 2-decylbenzothiophene (**12**) and 4-decyldibenzothiophene (**13**) are shown in Figures S9 and S10 of the Supporting Information, which stand for sulfur compounds with a monoalkyl chain. The single alkyl chain was easily cleaved at a collision energy of 30 V, leaving a CH_2 group on the aromatic ring. Significant loss of S was observed when the collision energy was above 50 V.

This work pays more attention to sulfur compounds with polyalkyl chains, and the tandem mass spectra of didodecyl alkylated dibenzothiophene (**14**) and trioctyl alkylated dibenzothiophene (**15**) are shown in Figures 10 and 11. Possible structures of fragment ions from compounds **14** are illustrated in Figure S11 of the Supporting Information. Partial fragmentations of the alkyl chains were observed at 30 V, resulting in two groups of fragment ions for compound **14** and three groups for compound **15**. Complete fragmentation was achieved at 50 V for compound **14** and 70 V for compound **15**. The loss of a S atom at a high collision energy was dramatically inhibited in compounds **14** and **15**, which was quite different from the S_1 model compounds with only one alkyl chain or

https://doi.org/10.1021/acs.energyfuels.1c03534
Energy Fuels 2022, 36, 1326−1337

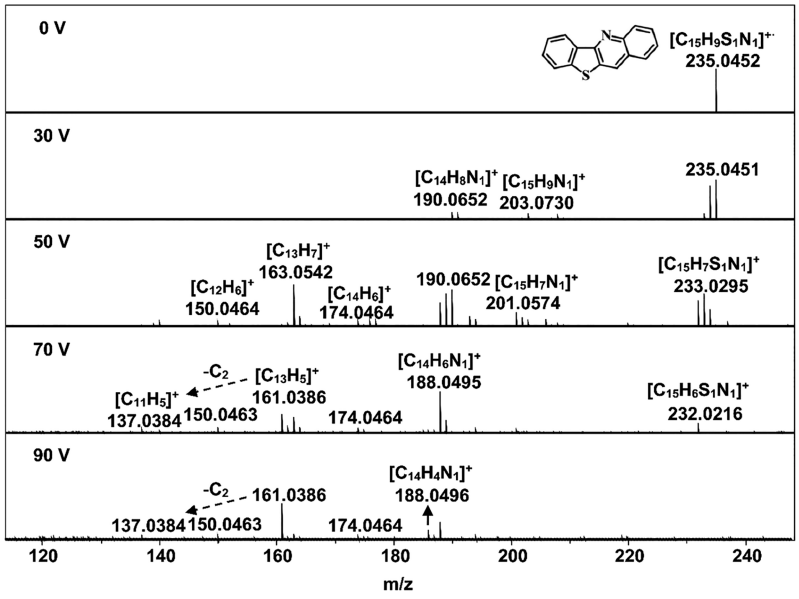

Figure 8. Tandem mass spectra of benzo[4,5]thieno[3,2-*b*]quinoline (**9**).

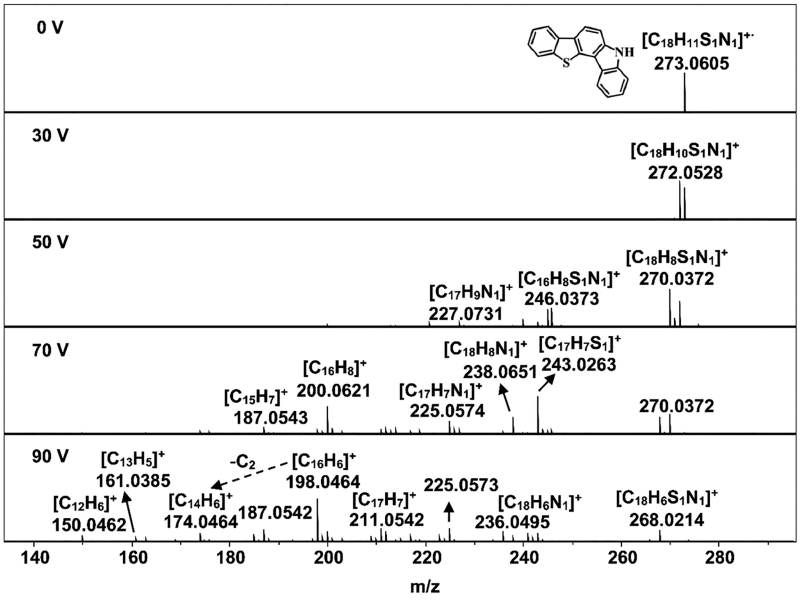

Figure 9. Tandem mass spectra of 5*H*-benzo[4,5]thieno[3,2-*c*]carbazole (**10**).

without any side chains. The fragment ion $[C_{12}H_8S_1]^+$ indicated the removal of all alkyl chains at high collision energies. However, the maximum carbon number of S_1 fragment ions still revealed the information of the initial structures, such as $[C_{15}H_9S_1]^+$ for compound **14** and $[C_{16}H_{10}S_1]^+$ for compound **15**, at 90 V. It was suspected that compounds with more side chains may generate fragment ions with a higher maximum carbon number at a high collision energy, which was also proven by didodecyl alkylated naphthalene (**A4**) and tridodecyl alkylated naphthalene (**A5**), as shown in Figures S12 and S13 of the Supporting Information. Besides, the C_2 losses were also observed for these model compounds with multiple alkyl side chains at high collision energies of 70 and 90 V.

3.4. Sulfur Compounds in an Atmospheric Residue and Its Hydrogenation Product. The broadband mass spectra of SA-AR and SA-AR-HT are shown in Figure S14 of the Supporting Information. The heteroatom class distributions of SA-AR and SA-AR-HT are shown in Figure S15a of the Supporting Information. S_1 species are the most dominant sulfur compounds in the feedstock and hydrogenation product. The DBE versus carbon number distributions of S_1 species are shown in Figure S15b of the Supporting Information. S_1 species with DBE lower than 9 are more likely to be removed after hydrotreatment, which is consistent with former reports.[36−39]

This work focuses on the structure differences of the same formula (such as $C_{40}H_{64}S_1$, m/z 576.4723) in the feedstock and product. The tandem mass spectra of SA-AR and SA-AR-HT with an isolation window of 576.4 ± 0.5 Da are shown in Figures S16 and S17 of the Supporting Information. The DBE versus carbon number distribution of fragment ions and

https://doi.org/10.1021/acs.energyfuels.1c03534
Energy Fuels 2022, 36, 1326−1337

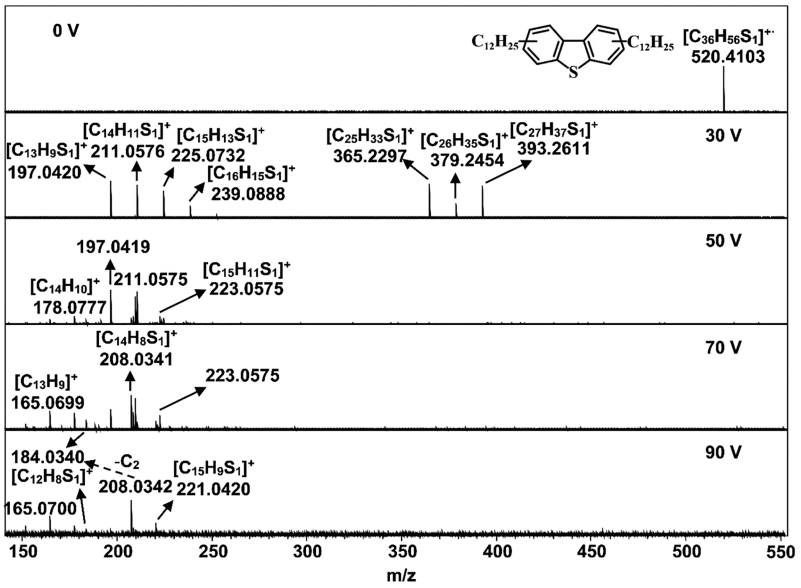

Figure 10. Tandem mass spectra of didodecyl alkylated dibenzothiophene (**14**).

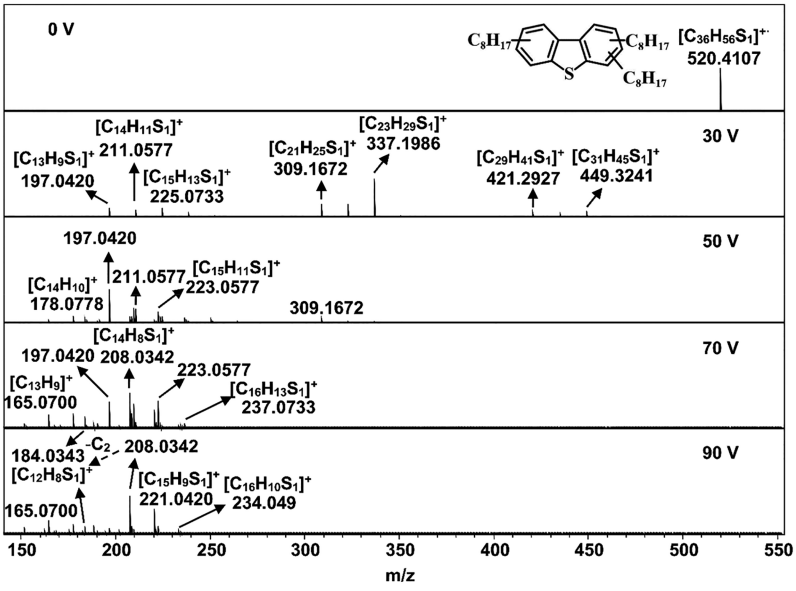

Figure 11. Tandem mass spectra of trioctyl alkylated dibenzothiophene (**15**).

corresponding parent ions for S_1 species in SA-AR and SA-AR-HT are shown in Figure 12. The isolation window is 576.4 ± 0.5 Da, and the collision energies are 30, 50, 70, and 90 V, respectively. The red bubbles present the parent ions ($C_{40}H_{64}S_1$, $C_{41}H_{52}S_1$, and $C_{42}H_{40}S_1$), and the blue bubbles present the fragment ions with odd m/z values. The distribution of fragment ions with even m/z values are shown in Figure S18 of the Supporting Information.

The CID spectra of S_1 species in SA-AR are shown in the left column of Figure 12. The opening of the naphthenic ring occurred at the collision energy of 30 V for model compound **1**. The bond lengths and bond energies of compound **1** and 2-butyldibenzothiophene were also compared and shown in Table S2 of the Supporting Information. It was found that the bond energies of C_α−C_β in compound **1** and 2-butyldibenzothiophene were at the same level, indicating that the opening of the naphthenic rings would be as easy as the cleavage of alkyl side chains. As a result, the opening of naphthenic rings was expected at a low collision energy of 30 V. Then, fragment ions with DBE of 6−8 at 30 V contributed to naphthenobenzothiophene, which was found in former reports.[73,74] The distributions of the fragment ions were continuous from the lowest carbon number to the carbon number of parent ions as a result of the partial cleavage of multiple side alkyl chains of sulfur compounds.[61] When the collision energy increased to 50 V, more side chains were cleaved. Significant C_2 losses occurred at a high collision energy of 70 V, indicating that most of the long side chains were cleaved. The largest carbon numbers of the fragment ions were labeled in the left column of Figure 12 for DBE = 9, 10, 16, and 17, which may be related to the number of side chains. When the collision energy increased to 90 V, the loss of the methyl group may emerge,[64]

https://doi.org/10.1021/acs.energyfuels.1c03534
Energy Fuels 2022, 36, 1326−1337

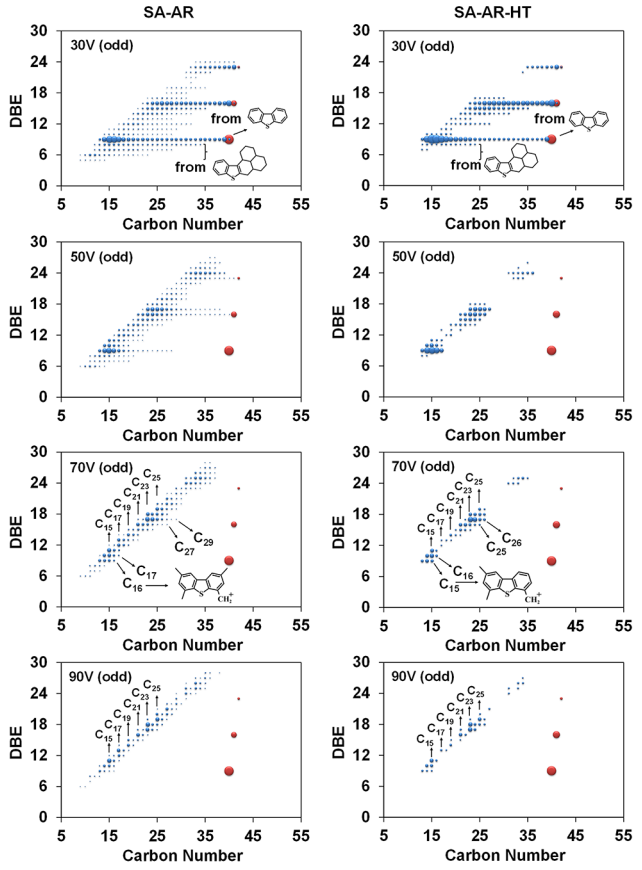

Figure 12. DBE versus carbon number distributions of S_1 species of SA-AR and SA-AR-HT. The isolation window is 576.4 ± 0.5 Da, and the collision energies are 30, 50, 70, and 90 V. The fragment ions with odd m/z are displayed in this figure.

which indicates that 90 V was not suitable to study the number of the side chains.

The CID spectra of S_1 species in SA-AR-HT are shown in the right column of Figure 12. At the collision energy of 30 V, the main difference between SA-AR and SA-AR-HT was that the relative abundance of fragment ions from naphthenobenzothiophene was reduced significantly in SA-AR-HT. When the collision energy increased to 70 V, the largest carbon numbers of the fragment ions of SA-AR-HT were all lower than those of SA-AR, indicating fewer alkyl chains in the sulfur compounds of the hydrogenation product. The differences between the carbon number distribution of the fragment ions have also been illustrated in Figure S19 of the Supporting Information.

From the combination of the information of sulfur compounds obtained from the CID spectra, the structural characters of $C_{40}H_{64}S_1$ before and after hydrogenation are suggested in Figure 13. Type A is dibenzothiophene-substituted with more alkyl chains; type B is dibenzothiophene-substituted with less alkyl chains; and types C and D are naphthenobenzothiophene with different numbers of alkyl chains. Types A and B have the same molecular formula, while the number of side chains in B is smaller. As a result, the average length of the side chains in B is much longer than that of A. The longer alkyl chains may have stronger steric hindrance during HDS of heavy oils. For types C and D, the existence of naphthenic rings reduces the planar structures dramatically, which facilitates the approach of sulfur compounds and HDS catalyst. Then, both C and D can be easily removed during the HDS process, regardless of the number of side chains.

Generally, the HDS process increases the content of naphthenic rings. It should be noted that most of the increased naphthenic rings exist in hydrocarbons instead of sulfur compounds. Sulfur compounds containing naphthenic rings in heavy oils are less resistant to HDS and easily transformed to aromatic hydrocarbons containing naphthenic rings, which is consistent with former reports.[14,73]

4. CONCLUSION

In this work, the CID spectra of a series of sulfur-containing model compounds were studied at different collision energies by FT-ICR MS. The loss of S atoms in the model compounds was suppressed at the collision energy of 30 V for S_1 model compounds, while significant removal of S atoms were achieved at collision energies higher than 50 V. For S_2 and S_3 model compounds, it was easy to lose one of the S atom at the collision energy of 30 V. With the increasing number of the aromatic rings in the sulfur-containing model compounds, the loss of the S atoms was restrained. The opening of the naphthenic ring in the sulfur model compound was observed at the collision energy of 30 V. Sulfur-containing model compounds attached with alkyl chains were also studied. It was found that partial cleavages of the multiple side chains were observed at the collision energy of 30 V, and complete cleavages were achieved at higher collision energies. The loss of S atoms was obviously inhibited at high collision energies

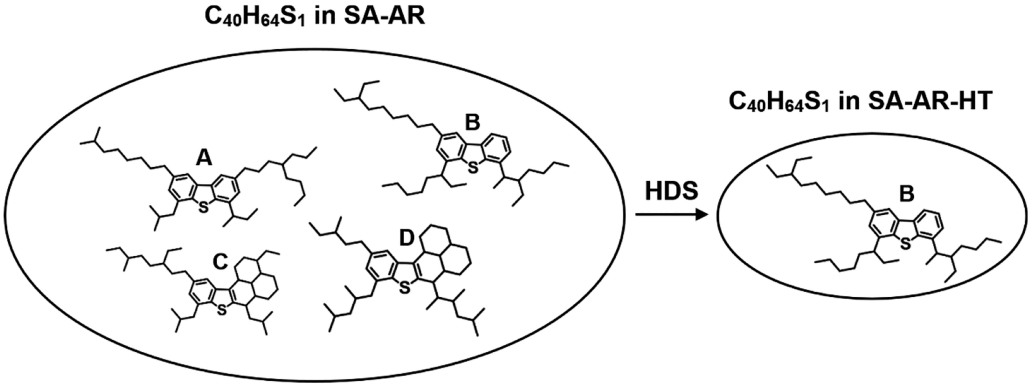

Figure 13. Possible structures of $C_{40}H_{64}S_1$ in the atmospheric residue (SA-AR) and its hydrogenation product (SA-AR-HT).

https://doi.org/10.1021/acs.energyfuels.1c03534
Energy Fuels 2022, 36, 1326−1337

for S_1 compounds with polyalkyl chains. The losses of the C_2 group were observed for most model compounds at high collision energies of 70 and 90 V.

On the basis of the fragmentation behaviors of the model compounds, the structure differences of the sulfur compounds in an atmospheric residue and its hydrogenation product were studied. The differences of naphthenic rings in sulfur compounds were compared at 30 V, and the differences of the numbers of side chains were compared at 70 V. The most refractory sulfur compounds in heavy oils during HDS contained fewer but longer alkyl side chains, and the ring structures were almost fully conjugated.

■ ASSOCIATED CONTENT

Supporting Information

The Supporting Information is available free of charge at https://pubs.acs.org/doi/10.1021/acs.energyfuels.1c03534.

Information of the aromatic model compounds (Table S1), bond energies for naphthenic and alkyl C−C bonds (Table S2), synthesis of alkylated dibenzothiophene and APPI FT-ICR MS spectra (Figure S1), tandem mass spectra of model compounds (Figures S2−S5, S8−S10, S12, and S13), possible structures of fragment ions from the model compounds (Figures S6, S7, and S11), and broadband mass spectra and tandem mass spectra of SA-AR and SA-AR-HT (Figures S14−S19) (PDF)

■ AUTHOR INFORMATION

Corresponding Author

Wei Wang − *SINOPEC Key Laboratory of Molecular Refining, SINOPEC Research Institute of Petroleum Processing, Beijing 100083, People's Republic of China;* orcid.org/0000-0002-6259-5471; Email: wangwei3.ripp@sinopec.com

Authors

Xinheng Cai − *SINOPEC Key Laboratory of Molecular Refining, SINOPEC Research Institute of Petroleum Processing, Beijing 100083, People's Republic of China*

Rong Shi − *SINOPEC Key Laboratory of Molecular Refining, SINOPEC Research Institute of Petroleum Processing, Beijing 100083, People's Republic of China*

Huandi Hou − *SINOPEC Key Laboratory of Molecular Refining, SINOPEC Research Institute of Petroleum Processing, Beijing 100083, People's Republic of China*

Dongyue Peng − *SINOPEC Key Laboratory of Molecular Refining, SINOPEC Research Institute of Petroleum Processing, Beijing 100083, People's Republic of China*

Naixin Wang − *SINOPEC Key Laboratory of Molecular Refining, SINOPEC Research Institute of Petroleum Processing, Beijing 100083, People's Republic of China;* orcid.org/0000-0001-5250-0902

Zhonghuo Deng − *SINOPEC Key Laboratory of Molecular Refining, SINOPEC Research Institute of Petroleum Processing, Beijing 100083, People's Republic of China*

Zelong Liu − *SINOPEC Key Laboratory of Molecular Refining, SINOPEC Research Institute of Petroleum Processing, Beijing 100083, People's Republic of China*

Qundan Zhang − *SINOPEC Key Laboratory of Molecular Refining, SINOPEC Research Institute of Petroleum Processing, Beijing 100083, People's Republic of China*

Complete contact information is available at: https://pubs.acs.org/10.1021/acs.energyfuels.1c03534

Notes

The authors declare no competing financial interest.

■ ACKNOWLEDGMENTS

This work was supported by the research project of SINOPEC (CLY19076) and the National Key Research and Development Program (2021YFA1501201). The authors gratefully acknowledge Prof. Jan T. Andersson and Prof. Qitao Tan for providing the sulfur-containing model compounds.

■ REFERENCES

(1) Han, Y.; Zhang, Y.; Xu, C.; Hsu, C. S. Molecular Characterization of Sulfur-Containing Compounds in Petroleum. *Fuel* **2018**, *221*, 144−158.

(2) Japes, A.; Penassa, M.; Andersson, J. T. Analysis of Recalcitrant Hexahydrodibenzothiophenes in Petroleum Products Using a Simple Fractionation Process. *Energy Fuels* **2009**, *23* (4), 2143−2148.

(3) Zhu, X.; Liu, M.; Liu, Z.; Li, Y.; Tian, S. Direct and Rapid Quantitative Analysis of Alkyldibenzothiophenes in Deeply Hydrodesulfurized Diesel Fuel by Gas Chromatography Quadrupole Time-of-Flight Mass Spectrometry. *Energy Fuels* **2017**, *31* (9), 9125−9131.

(4) Choudhary, T. V.; Malandra, J.; Green, J.; Parrott, S.; Johnson, B. Towards Clean Fuels: Molecular-Level Sulfur Reactivity in Heavy Oils. *Angew. Chem.* **2006**, *118* (20), 3377−3381.

(5) Choudhary, T. V. Structure-Reactivity-Mechanistic Considerations in Heavy Oil Desulfurization. *Ind. Eng. Chem. Res.* **2007**, *46* (25), 8363−8370.

(6) Choudhary, T. V.; Parrott, S.; Johnson, B. Unraveling Heavy Oil Desulfurization Chemistry: Targeting Clean Fuels. *Environ. Sci. Technol.* **2008**, *42* (6), 1944−1947.

(7) Bataille, F.; Lemberton, J. L.; Michaud, P.; Pérot, G.; Vrinat, M.; Lemaire, M.; Schulz, E.; Breysse, M.; Kasztelan, S. Alkyldibenzothiophenes Hydrodesulfurization-Promoter Effect, Reactivity, and Reaction Mechanism. *J. Catal.* **2000**, *191* (2), 409−422.

(8) van Haandel, L.; Bremmer, M.; Kooyman, P. J.; van Veen, J. A. R.; Weber, T.; Hensen, E. J. M. Structure−Activity Correlations in Hydrodesulfurization Reactions over Ni-Promoted $Mo_xW_{(1-x)}S_2/Al_2O_3$ Catalysts. *ACS Catal.* **2015**, *5* (12), 7276−7287.

(9) Wu, L.; Liu, Y.; Zhang, Q. Operational Optimization of a Hydrotreating System Based on Removal of Sulfur Compounds in Hydrotreaters Coupled with a Fluid Catalytic Cracker. *Energy Fuels* **2017**, *31* (9), 9850−9862.

(10) Shih, S. S.; Mizrahi, S.; Green, L. A.; Sarli, M. S. Deep Desulfurization of Distillates. *Ind. Eng. Chem. Res.* **1992**, *31* (4), 1232−1235.

(11) Kabe, T.; Ishihara, A.; Tajima, H. Hydrodesulfurization of Sulfur-Containing Polyaromatic Compounds in Light Oil. *Ind. Eng. Chem. Res.* **1992**, *31* (6), 1577−1580.

(12) Rodgers, R. P.; White, F. M.; Hendrickson, C. L.; Marshall, A. G.; Andersen, K. V. Resolution, Elemental Composition, and Simultaneous Monitoring by Fourier Transform Ion Cyclotron Resonance Mass Spectrometry of Organosulfur Species before and after Diesel Fuel Processing. *Anal. Chem.* **1998**, *70* (22), 4743−4750.

(13) Schade, T.; Andersson, J. T. Speciation of Alkylated Dibenzothiophenes in a Deeply Desulfurized Diesel Fuel. *Energy Fuels* **2006**, *20* (4), 1614−1620.

(14) Ma, X.; Sakanishi, K.; Isoda, T.; Mochida, I. Quantum Chemical Calculation on the Desulfurization Reactivities of Heterocyclic Sulfur Compounds. *Energy Fuels* **1995**, *9* (1), 33−37.

(15) Mahé, L.; Dutriez, T.; Courtiade, M.; Thiébaut, D.; Dulot, H.; Bertoncini, F. Global Approach for the Selection of High Temperature Comprehensive Two-Dimensional Gas Chromatography Experimental Conditions and Quantitative Analysis in Regards to Sulfur-Containing Compounds in Heavy Petroleum Cuts. *J. Chromatogr. A* **2011**, *1218* (3), 534−544.

(16) Machado, M. E.; Bregles, L. P.; de Menezes, E. W.; Caramão, E. B.; Benvenutti, E. V.; Zini, C. A. Comparison between Pre-fractionation and Fractionation Process of Heavy Gas Oil for Determination of Sulfur Compounds Using Comprehensive Two-Dimensional Gas Chromatography. *J. Chromatogr. A* **2013**, *1274*, 165−172.
(17) Franchina, F. A.; Machado, M. E.; Tranchida, P. Q.; Zini, C. A.; Caramão, E. B.; Mondello, L. Determination of Aromatic Sulphur Compounds in Heavy Gas Oil by Using (Low-)Flow Modulated Comprehensive Two-Dimensional Gas Chromatography−Triple Quadrupole Mass Spectrometry. *J. Chromatogr. A* **2015**, *1387*, 86−94.
(18) Lorentz, C.; Laurenti, D.; Zotin, J. L.; Geantet, C. Comprehensive GC × GC Chromatography for the Characterization of Sulfur Compound in Fuels: A Review. *Catal. Today* **2017**, *292*, 26−37.
(19) Byer, J. D.; Siek, K.; Jobst, K. Distinguishing the C_3 vs SH_4 Mass Split by Comprehensive Two-Dimensional Gas Chromatography−High Resolution Time-of-Flight Mass Spectrometry. *Anal. Chem.* **2016**, *88* (12), 6101−6104.
(20) Jennerwein, M. K.; Eschner, M. S.; Wilharm, T.; Zimmermann, R.; Gröger, T. M. Proof of Concept of High-Temperature Comprehensive Two-Dimensional Gas Chromatography Time-of-Flight Mass Spectrometry for Two-Dimensional Simulated Distillation of Crude Oils. *Energy Fuels* **2017**, *31* (11), 11651−11659.
(21) Lobodin, V. V.; Robbins, W. K.; Lu, J.; Rodgers, R. P. Separation and Characterization of Reactive and Non-Reactive Sulfur in Petroleum and Its Fractions. *Energy Fuels* **2015**, *29* (10), 6177−6186.
(22) Cho, Y.; Birdwell, J. E.; Hur, M.; Lee, J.; Kim, B.; Kim, S. Extension of the Analytical Window for Characterizing Aromatic Compounds in Oils Using a Comprehensive Suite of High-Resolution Mass Spectrometry Techniques and Double Bond Equivalence versus Carbon Number Plot. *Energy Fuels* **2017**, *31* (8), 7874−7883.
(23) Niyonsaba, E.; Manheim, J. M.; Yerabolu, R.; Kenttamaa, H. I. Recent Advances in Petroleum Analysis by Mass Spectrometry. *Anal. Chem.* **2019**, *91* (1), 156−177.
(24) Purcell, J. M.; Juyal, P.; Kim, D. G.; Rodgers, R. P.; Hendrickson, C. L.; Marshall, A. G. Sulfur Speciation in Petroleum: Atmospheric Pressure Photoionization or Chemical Derivatization and Electrospray Ionization Fourier Transform Ion Cyclotron Resonance Mass Spectrometry. *Energy Fuels* **2007**, *21* (5), 2869−2874.
(25) Cho, Y.; Kim, Y. H.; Kim, S. Planar Limit-Assisted Structural Interpretation of Saturates/Aromatics/Resins/Asphaltenes Fractionated Crude Oil Compounds Observed by Fourier Transform Ion Cyclotron Resonance Mass Spectrometry. *Anal. Chem.* **2011**, *83* (15), 6068−6073.
(26) Corilo, Y. E.; Rowland, S. M.; Rodgers, R. P. Calculation of the Total Sulfur Content in Crude Oils by Positive-Ion Atmospheric Pressure Photoionization Fourier Transform Ion Cyclotron Resonance Mass Spectrometry. *Energy Fuels* **2016**, *30* (5), 3962−3966.
(27) Son, S.; Kim, S.; Yim, Y. H.; Kim, S. Reproducibility of Crude Oil Spectra Obtained with Ultrahigh Resolution Mass Spectrometry. *Anal. Chem.* **2020**, *92* (14), 9465−9471.
(28) Muller, H.; Alawani, N. A.; Adam, F. M. Innate Sulfur Compounds as an Internal Standard for Determining Vacuum Gas Oil Compositions by APPI FT-ICR MS. *Energy Fuels* **2020**, *34* (7), 8260−8273.
(29) Müller, H.; Andersson, J. T.; Schrader, W. Characterization of High-Molecular-Weight Sulfur-Containing Aromatics in Vacuum Residues Using Fourier Transform Ion Cyclotron Resonance Mass Spectrometry. *Anal. Chem.* **2005**, *77* (8), 2536−2543.
(30) Shi, Q.; Pan, N.; Liu, P.; Chung, K. H.; Zhao, S.; Zhang, Y.; Xu, C. Characterization of Sulfur Compounds in Oilsands Bitumen by Methylation Followed by Positive-Ion Electrospray Ionization and Fourier Transform Ion Cyclotron Resonance Mass Spectrometry. *Energy Fuels* **2010**, *24* (5), 3014−3019.
(31) Lobodin, V. V.; Juyal, P.; McKenna, A. M.; Rodgers, R. P.; Marshall, A. G. Silver Cationization for Rapid Speciation of Sulfur-Containing Species in Crude Oils by Positive Electrospray Ionization Fourier Transform Ion Cyclotron Resonance Mass Spectrometry. *Energy Fuels* **2014**, *28* (1), 447−452.
(32) Ni, H.; Xu, C.; Wang, R.; Guo, X.; Long, Y.; Ma, C.; Yan, L.; Liu, X.; Shi, Q. Composition and Transformation of Sulfur-, Oxygen-, and Nitrogen-Containing Compounds in the Hydrotreating Process of a Low-Temperature Coal Tar. *Energy Fuels* **2018**, *32* (3), 3077−3084.
(33) Zhang, K.; Yu, J.; Gao, S.; Li, C.; Xu, G. Understanding Shale Oil Hydrotreatment with Composition Analysis Using Positive-Ion Mode Atmospheric Pressure Photoionization Fourier Transform Ion Cyclotron Resonance Mass Spectrometry. *Energy Fuels* **2017**, *31* (2), 1362−1369.
(34) Klein, G. C.; Rodgers, R. P.; Marshall, A. G. Identification of Hydrotreatment-Resistant Heteroatomic Species in a Crude Oil Distillation Cut by Electrospray Ionization FT-ICR Mass Spectrometry. *Fuel* **2006**, *85* (14−15), 2071−2080.
(35) Guillemant, J.; Berlioz-Barbier, A.; Chainet, F.; de Oliveira, L. P.; Lacoue-Nègre, M.; Joly, J.-F.; Duponchel, L. Sulfur Compounds Characterization Using FT-ICR MS: Towards a Better Comprehension of Vacuum Gas Oils Hydrodesulfurization Process. *Fuel Process. Technol.* **2020**, *210*, 106529.
(36) Liu, M.; Wang, M.; Zhang, L.; Xu, Z.; Chen, Y.; Guo, X.; Zhao, S. Transformation of Sulfur Compounds in the Hydrotreatment of Supercritical Fluid Extraction Subfractions of Saudi Arabia Atmospheric Residua. *Energy Fuels* **2015**, *29* (2), 702−710.
(37) Zhang, C.; Zhang, Y.; Liu, M.; Guan, Y. M.; Yuan, S. H. Transformation of Sulfur Compounds in Two Typical Atmospheric Residues in Hydrotreating via ESI FT-ICR MS. *Fuel* **2020**, *281*, 118731.
(38) Zhao, J.; Liu, T.; Han, W.; Ren, L.; Zhang, L.; Dai, L.; Li, D. An Insight into the Molecular Structure of Sulfur Compounds and Their Reactivity during Residual Oil Hydroprocessing. *Fuel* **2021**, *283*, 119334.
(39) Zhao, J.; Dai, L.; Wang, W.; Liu, T.; Ren, L.; Zhang, L.; Han, W.; Li, D. Unraveling the Molecular-Level Structures and Distribution of Refractory Sulfur Compounds During Residue Hydrotreating Process. *Fuel Process. Technol.* **2021**, *224*, 107025.
(40) Cho, E.; Cho, Y.; Rakhmat, S.; Kim, Y. H.; Kim, S. Molecular-Level Structural Analysis of Hydrotreated and Untreated Atmospheric Residue Oils via Atmospheric Pressure Photoionization Cyclic Ion Mobility Mass Spectrometry and Ultrahigh-Resolution Mass Spectrometry. *Energy Fuels* **2021**, *35* (22), 18163−18169.
(41) Purcell, J. M.; Merdrignac, I.; Rodgers, R. P.; Marshall, A. G.; Gauthier, T.; Guibard, I. Stepwise Structural Characterization of Asphaltenes during Deep Hydroconversion Processes Determined by Atmospheric Pressure Photoionization (APPI) Fourier Transform Ion Cyclotron Resonance (FT-ICR) Mass Spectrometry. *Energy Fuels* **2010**, *24* (4), 2257−2265.
(42) Jin, N.; Wang, G.; Han, S.; Meng, Y.; Xu, C.; Gao, J. Hydroconversion Behavior of Asphaltenes under Liquid-Phase Hydrogenation Conditions. *Energy Fuels* **2016**, *30* (4), 2594−2603.
(43) Rogel, E.; Witt, M. Asphaltene Characterization during Hydroprocessing by Ultrahigh-Resolution Fourier Transform Ion Cyclotron Resonance Mass Spectrometry. *Energy Fuels* **2017**, *31* (4), 3409−3416.
(44) Panda, S. K.; Alawani, N. A.; Lajami, A. R.; Al-Qunaysi, T. A.; Muller, H. Characterization of Aromatic Hydrocarbons and Sulfur Heterocycles in Saudi Arabian Heavy Crude Oil by Gel Permeation Chromatography and Ultrahigh Resolution Mass Spectrometry. *Fuel* **2019**, *235*, 1420−1426.
(45) Santos de Freitas, C.; Valencia-Dávila, J. A.; Lopes Pereira, R. C.; Torres Abrantes, L.; Kato, L.; Gontijo Vaz, B. Isolation and Characterization of Sulfur-Containing Compounds by Positive-Ion Electrospray Ionization and Online HPLC/Atmospheric Pressure Chemical Ionization Coupled to Orbitrap Mass Spectrometry. *Fuel* **2021**, *289*, 119783.
(46) Vetere, A.; Pröfrock, D.; Schrader, W. Qualitative and Quantitative Evaluation of Sulfur-Containing Compound Types in

https://doi.org/10.1021/acs.energyfuels.1c03534
Energy Fuels 2022, 36, 1326−1337

Heavy Crude Oil and Its Fractions. *Energy Fuels* **2021**, *35* (10), 8723−8732.
(47) Rüger, C. P.; Neumann, A.; Sklorz, M.; Schwemer, T.; Zimmermann, R. Thermal Analysis Coupled to Ultra High Resolution Mass Spectrometry with Collision Induced Dissociation for Complex Petroleum Samples − Heavy Oil Composition and Asphaltene Precipitation Effects. *Energy Fuels* **2017**, *31* (12), 13144−13158.
(48) Rüger, C. P.; Grimmer, C.; Sklorz, M.; Neumann, A.; Streibel, T.; Zimmermann, R. Combination of Different Thermal Analysis Methods Coupled to Mass Spectrometry for the Analysis of Asphaltenes and Their Parent Crude Oils: Comprehensive Characterization of the Molecular Pyrolysis Pattern. *Energy Fuels* **2018**, *32* (3), 2699−2711.
(49) Neumann, A.; Käfer, U.; Gröger, T.; Wilharm, T.; Zimmermann, R.; Rüger, C. P. Investigation of Aging Processes in Bitumen at the Molecular Level with High-Resolution Fourier-Transform Ion Cyclotron Mass Spectrometry and Two-Dimensional Gas Chromatography Mass Spectrometry. *Energy Fuels* **2020**, *34* (9), 10641−10654.
(50) Ahmed, A.; Cho, Y. J.; No, M.; Koh, J.; Tomczyk, N.; Giles, K.; Yoo, J. S.; Kim, S. Application of the Mason-Schamp Equation and Ion Mobility Mass Spectrometry to Identify Structurally Related Compounds in Crude Oil. *Anal. Chem.* **2011**, *83* (1), 77−83.
(51) Maire, F.; Neeson, K.; Denny, R.; McCullagh, M.; Lange, C.; Afonso, C.; Giusti, P. Identification of Ion Series Using Ion Mobility Mass Spectrometry: The Example of Alkyl-Benzothiophene and Alkyl-Dibenzothiophene Ions in Diesel Fuels. *Anal. Chem.* **2013**, *85* (11), 5530−5534.
(52) Maleki, H.; Ghassabi Kondalaji, S.; Khakinejad, M.; Valentine, S. J. Structural Assignments of Sulfur-Containing Compounds in Crude Oil Using Ion Mobility Spectrometry-Mass Spectrometry. *Energy Fuels* **2016**, *30* (11), 9150−9161.
(53) Cho, E.; Riches, E.; Palmer, M.; Giles, K.; Ujma, J.; Kim, S. Isolation of Crude Oil Peaks Differing by $m/z \sim 0.1$ via Tandem Mass Spectrometry Using a Cyclic Ion Mobility-Mass Spectrometer. *Anal. Chem.* **2019**, *91* (22), 14268−14274.
(54) Zhang, Y.; Han, Y.; Wu, J.; Wang, Y.; Li, J.; Shi, Q.; Xu, C.; Hsu, C. S. Comprehensive Composition, Structure, and Size Characterization for Thiophene Compounds in Petroleum Using Ultrahigh-Resolution Mass Spectrometry and Trapped Ion Mobility Spectrometry. *Anal. Chem.* **2021**, *93* (12), 5089−5097.
(55) Qian, K.; Edwards, K. E.; Mennito, A. S.; Freund, H.; Saeger, R. B.; Hickey, K. J.; Francisco, M. A.; Yung, C.; Chawla, B.; Wu, C.; Kushnerick, J. D.; Olmstead, W. N. Determination of Structural Building Blocks in Heavy Petroleum Systems by Collision-Induced Dissociation Fourier Transform Ion Cyclotron Resonance Mass Spectrometry. *Anal. Chem.* **2012**, *84* (10), 4544−4551.
(56) Podgorski, D. C.; Corilo, Y. E.; Nyadong, L.; Lobodin, V. V.; Bythell, B. J.; Robbins, W. K.; McKenna, A. M.; Marshall, A. G.; Rodgers, R. P. Heavy Petroleum Composition. 5. Compositional and Structural Continuum of Petroleum Revealed. *Energy fuels* **2013**, *27* (3), 1268−1276.
(57) Teratani, S.; Katano, K.; Tanaka, R.; Nakamura, T.; Inomata, H. Core Structure Analysis of Heavy Oil Components with Fourier Transform Ion Cyclotron Resonance Mass Spectrometry. *J. Jpn. Pet. Inst.* **2019**, *62* (6), 272−281.
(58) Hunt, D. F.; Shabanowitz, J. Determination of Organosulfur Compounds in Hydrocarbon Matrixes by Collision Activated Dissociation Mass Spectrometry. *Anal. Chem.* **1982**, *54* (3), 574−578.
(59) Herrera, L. C.; Ramaley, L.; Grossert, J. S. Fragmentation Pathways of Some Benzothiophene Radical Cations Formed by Atmospheric Pressure Chemical Ionisation. *Rapid Commun. Mass Spectrom.* **2009**, *23* (5), 571−579.
(60) Tang, W.; Sheng, H.; Jin, C.; Riedeman, J. S.; Kenttämaa, H. I. Characterization of Aromatic Organosulfur Model Compounds Relevant to Fossil Fuels by Using Atmospheric Pressure Chemical Ionization with CS_2 and High-Resolution Tandem Mass Spectrometry. *Rapid Commun. Mass Spectrom.* **2016**, *30* (7), 953−962.
(61) Vetere, A.; Alachraf, M. W.; Panda, S. K.; Andersson, J. T.; Schrader, W. Studying the Fragmentation Mechanism of Selected Components Present in Crude Oil by Collision-Induced Dissociation Mass Spectrometry. *Rapid Commun. Mass Spectrom.* **2018**, *32* (24), 2141−2151.
(62) Qian, K.; Edwards, K. E.; Mennito, A. S.; Freund, H. Determination of Cores or Building Blocks and Reconstruction of Parent Molecules in Heavy Petroleums and Other Hydrocarbon Resources. U.S. Patent 20120156798 A1, June 21, 2012.
(63) Liu, L.; Song, C.; Tian, S.; Zhang, Q.; Cai, X.; Liu, Y.; Liu, Z.; Wang, W. Structural Characterization of Sulfur-Containing Aromatic Compounds in Heavy Oils by FT-ICR Mass Spectrometry with a Narrow Isolation Window. *Fuel* **2019**, *240*, 40−48.
(64) Jarrell, T. M.; Jin, C.; Riedeman, J. S.; Owen, B. C.; Tan, X.; Scherer, A.; Tykwinski, R. R.; Gray, M. R.; Slater, P.; Kenttämaa, H. I. Elucidation of Structural Information Achievable for Asphaltenes via Collision-Activated Dissociation of Their Molecular Ions in MS^n Experiments: A Model Compound Study. *Fuel* **2014**, *133*, 106−114.
(65) Ha, J.; Cho, E.; Kim, S. Interpreting Chemical Structures of Compounds in Crude Oil Based on the Tandem Mass Spectra of Standard Compounds Obtained at the Same Normalized Collision Energy. *Energy Fuels* **2017**, *31* (7), 6960−6967.
(66) Nyadong, L.; Lai, J.; Thompsen, C.; Lafrancois, C. J.; Cai, X.; Song, C.; Wang, J.; Wang, W. High-Field Orbitrap Mass Spectrometry and Tandem Mass Spectrometry for Molecular Characterization of Asphaltenes. *Energy Fuels* **2018**, *32* (1), 294−305.
(67) Wittrig, A. M.; Fredriksen, T. R.; Qian, K.; Clingenpeel, A. C.; Harper, M. R. Single Dalton Collision-Induced Dissociation for Petroleum Structure Characterization. *Energy Fuels* **2017**, *31* (12), 13338−13344.
(68) Zhang, T.; Deng, G.; Li, H.; Liu, B.; Tan, Q.; Xu, B. Cyclization of 2-Biphenylthiols to Dibenzothiophenes under $PdCl_2$/DMSO Catalysis. *Org. Lett.* **2018**, *20* (17), 5439−5443.
(69) Luong, B. X.; Petre, A. L.; Hoelderich, W. F.; Commarieu, A.; Laffitte, J. A.; Espeillac, M.; Souchet, J. C. Use of Methanesulfonic Acid as Catalyst for the Production of Linear Alkylbenzenes. *J. Catal.* **2004**, *226* (2), 301−307.
(70) Santos, V. G.; Fasciotti, M.; Pudenzi, M. A.; Klitzke, C. F.; Nascimento, H. L.; Pereira, R. C. L.; Bastos, W. L.; Eberlin, M. N. Fullerenes in Asphaltenes and Other Carbonaceous Materials: Natural Constituents or Laser Artifacts? *Analyst* **2016**, *141* (9), 2767−2773.
(71) Li, M.; Wang, H.; Shi, S.; Fang, R.; Tang, Q.; Wang, D. The Occurrence and Distribution of Phenylnaphthalenes, Terphenyls and Quaterphenyls in Selected Lacustrine Shales and Related Oils in China. *Org. Geochem.* **2016**, *95*, 55−70.
(72) Chacón-Patiño, M. L.; Rowland, S. M.; Rodgers, R. P. Advances in Asphaltene Petroleomics. Part 1: Asphaltenes Are Composed of Abundant Island and Archipelago Structural Motifs. *Energy Fuels* **2017**, *31* (12), 13509−13518.
(73) Nolte, T.; Posch, T. N.; Huhn, C.; Andersson, J. T. Desulfurized Fuels from Athabasca Bitumen and Their Polycyclic Aromatic Sulfur Heterocycles. Analysis Based on Capillary Electrophoresis Coupled with TOF MS. *Energy Fuels* **2013**, *27* (1), 97−107.
(74) Wu, J.; Zhang, W.; Ma, C.; Wang, F.; Zhou, X.; Chung, K. H.; Hou, D.; Zhang, Y.; Shi, Q. Isolation and Characterization of Sulfur Compounds in a Lacustrine Crude Oil. *Fuel* **2019**, *253*, 1482−1489.
(75) Girgis, M. J.; Gates, B. C. Reactivities, Reaction Networks, and Kinetics in High-Pressure Catalytic Hydroprocessing. *Ind. Eng. Chem. Res.* **1991**, *30* (9), 2021−2058.

NOTE ADDED AFTER ASAP PUBLICATION

This article originally published with the two images at the bottom of Figure 12 reversed. The corrected figure published January 25, 2022.

https://doi.org/10.1021/acs.energyfuels.1c03534
Energy Fuels 2022, 36, 1326−1337